

The Gouy-Chapman Capacitor of Double Layer in Dye Sensitized Solar Cells: Study and Simulation

Toufik ATOUANI*[‡], Abdelkader SAIDANE**, Abdelkader NOURI*, Azeddine ZOUADI*

*Department of Material Sciences, Faculty of Exact Sciences, Mohammed TAHRI University, BP 417, Bechar, Algeria.

**CaSiCCE Laboratory, BP 1523 El M'Naouar 31000, ENP-Oran, Algeria.

(toufikatouani1972@yahoo.fr, saidaneak@yahoo.com, nouri_32@yahoo.fr, zouaidiazzeddine@yahoo.fr)

[‡] Corresponding Author; Toufik ATOUANI, Department of Material Sciences, Faculty of Exact Sciences, Mohammed TAHRI University, BP 417, Bechar, Algeria,

Tel: +213 49238993, Fax: +213 49238974, toufikatouani1972@yahoo.fr

Received: 06.01.2016 Accepted: 16.02.2016

Abstract- In this paper, we investigate the effect of the Gouy-Chapman capacitor (C_{gc}) created at electrolyte/counter electrode interface in the Dye Sensitized Solar Cells (DSSC) on its J-V curve. For this purpose, an adequate electrical model was developed. This model is based on the theory of double layer in electrolyte/metal interface. The results show that by increasing the ions concentration in the electrolyte, the C_{gc} is increased improving the Maximum Power Point (MPP) and the efficiency of about 10%. On the other hand the J-V curve deteriorates by increasing the frequency of periodic shading above 0.03 Hz.

Keywords Dye Sensitized Solar Cells (DSSC) - Double Layer - Gouy-Chapman's capacitor (C_{gc}), J-V curve.

1. Introduction

In last three decades, there has been an important development of DSSC based on regenerative photo-electrochemical principles [1-4]. Most studies in this field have neglected the effect of double layer at electrolyte/metal contact [5,6].

Most parts of the photovoltaic effect phenomena involved in the DSSC (the light absorption, photo-generation, regeneration of dye and the separation of charge carriers) are located in the active layer that extends from 10 μm to 20 μm from the electrode [7]. The oxidized mediator (I_3^-) in the electrolyte is transported to the counter electrode where their regeneration occurs by the electrons through the external circuit. The C_{gc} is created at the electrolyte/metal interface, the charge carriers transfer is influenced by this C_{gc} . This phenomenon was neglected in most previous studies [8, 9].

In the present work the influence of electrolyte/metal interface at the counter electrode and the impact of the

periodic shading of light flow on the solar cells J-V curve will be investigated.

2. Theoretical model

2.1. Metal electrolyte interface

The corrosion of metallic materials in an aqueous medium involves reactions between the metal (the electrode) and the solution (the electrolyte), which occur at the interface between the two media.

Metal is considered as a globally neutral compound formed by positive ions occupying the positions of the crystal lattice and mobile electrons [10]. Despite this mobility, the electrons can move away to a great distance from the crystal because the positive nucleus exerts an attractive force. However, in the absence of external environment, the surface of a metallic material is considered as the superposition of two thin layers; one positively charged below the surface of the

solid and the other negatively charged adjacent on the surface [7].

This charge separation zone constitutes the electrical double layer [11] (Figure 1).

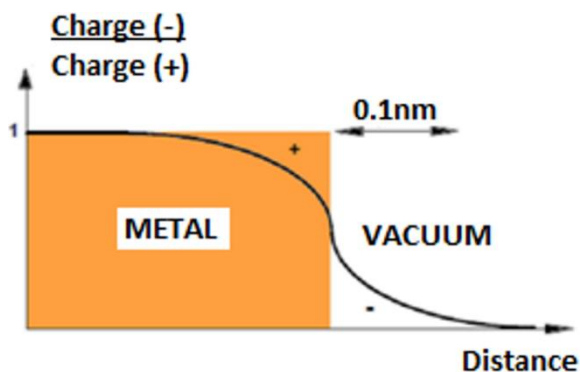


Fig. 1. Electric double layer on metal surface [11]

When metal is in contact with an electrolyte, there is also a separation of electrical charges. Their distribution at the interface depends on the adsorption of water molecules or hydrated cations as well as chemical adsorption anion to the metal surface. According to the applied potential, the charge of the metal can be positive or negative with respect to that of the electrolyte. The composition of the double layer, thus also depends on this potential; still the electrical neutrality condition is always respected [11].

Since water consists of dipole molecules, their adsorption on the surface of a metal, is guided by the charges present at the surface. Dissolved cations are generally hydrated, they must not get in touch with the surface; a distance less than the radius of the hydrated sphere separates them (Figure 2) [12]. The anions are rarely hydrated. They can be chemically adsorbed on the metal surface, even if they are negatively charged, and thus, replace water molecules [12]. An example of this type of interface is shown in Figure 2.

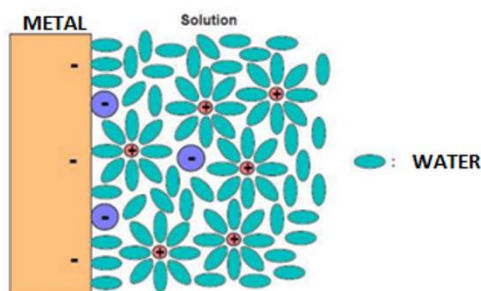


Fig. 2. Diagram of double layer metal/solution interface [12]

2.2. Electrical analogy of the double layer

2.2.1. Electrical equivalent circuit

The double layer corresponds, by definition, to the electrode/electrolyte interface where charge separation occurs. Its electrical behaviour can be likened to that of an assembly of the capacitor C (called double layer capacitor)

connected in parallel with the resistor R_t (called transfer resistor) according to the simple diagram shown in Figure 3.

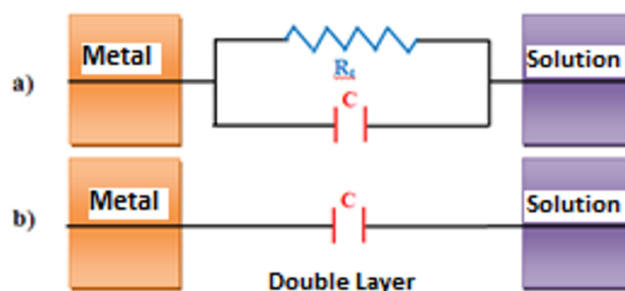
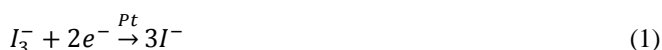


Fig. 3. Electric equivalent circuit of electrode/electrolyte interface:

- (a) Capacity of double layer and the charge transfer resistor – real case-;
- (b) Polarizable electrode, charge transfer resistor is infinite – ideal case-

The diagram of Figure 3 shows that a direct current can pass through the metal/solution interface. This current, called current transfer or load current Faraday, is the result of the electrochemical reaction which occurs at the interface (charge transfer reaction at Pt counter electrode) equation (1).



Some metal/solution pairs (e.g. Hg/NaCl) contain substantially no reactive species. Therefore, they allow the variation of the potential difference at the terminals of the equivalent circuit with no current flows through it [13]. This corresponds to an infinite value of the R_t in the scheme, hence the system that has this property is an ideally polarizable electrode. Note that the electrode includes both the material and solution.

Several theoretical models have been developed to account for the electrical properties of the double layer [12]. In the following section the Gouy-Chapman model will be briefly illustrated. The choice of this model is justified because it is appropriate for low solution electrolyte concentration; the experimental case of electrolyte of DSSC [14].

2.2.2. Model of Gouy-Chapman

In Gouy-Chapman model, the ions in solution do not occupy a fixed position in a plan. They are distributed in a statistical Boltzmann distribution in a region near the metal surface called diffuse double layer, or layer of Gouy-Chapman (L_{GC}) (Figure 4) [13].

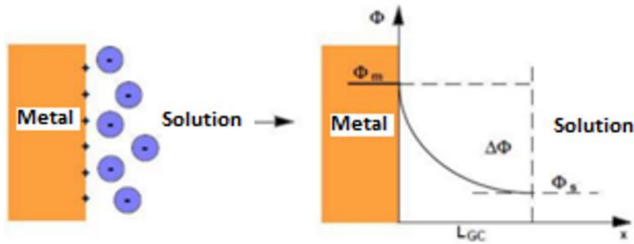


Fig. 4. Gouy-Chapman double layer model.

The width of this area L_{GC} can be of the order of 30 nm, well above the Helmholtz double layer [7].

In the Helmholtz model Figure 5, the double layer is treated as a plan capacitor whose capacitance C_H can be calculated using equation (2):

$$C_H = \frac{\epsilon_{H_2O} \epsilon_0}{L_H} = \frac{dq}{d\Delta\Phi} \quad (2)$$

Where ϵ_{H_2O} represents the dielectric constant of water (in case the solvent is water), ϵ_0 : permittivity constant (Fm^{-1}), q : the charge density in the double layer ($C.m^{-2}$), $\Delta\Phi$: the potential difference (V) across the double layer ($\Delta\Phi = \Phi_m - \Phi_s$) and L_H : capacitor thickness (m) as shown in Figure 5.

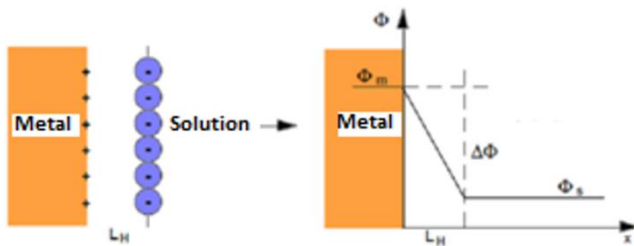


Fig. 5. Helmholtz double layer model

In this model and according to equation (2) the potential difference and the charge density are connected, the double layer capacitance of the Helmholtz model does not depend on potential or species in solution.

The double layer capacity may in some cases depend on the concentration of ions in the electrolyte. This behaviour, observed in particular for low-concentrated solutions, results from the thermal motion of the ions [15].

Considering the distribution of ions governed by Boltzmann statistics, the double layer capacitance, according to the Gouy-Chapman model, is obtained by the following equations [15]:

$$C_{GC} = \left(\frac{\epsilon_{H_2O} \epsilon_0}{L_{GC}} \right) \cosh \left(\frac{zF\Delta\Phi}{2RT} \right) \quad (3)$$

with

$$L_{GC} = \left(\frac{\epsilon_{H_2O} \epsilon_0 RT}{2F^2 z^2 C} \right) \cosh \left(\frac{zF\Delta\Phi}{2RT} \right) \quad (4)$$

Where z and C , respectively, represent the charge and concentration of ions in solution, F represents the electric charge of one mole of electrons (96500 C), T : Ambient temperature [K].

The variation of potential within the layer is represented by the following equation:

$$\Phi(x) = \Phi_m \exp\left(-\frac{x}{L_{GC}}\right) \quad (5)$$

Φ_m represents the metal maximum potential. The Gouy-Chapman theory also applies to insulating materials. Instead of Φ_m potential corresponding to the value $x = 0$, this case is called "zeta potential" Φ_ξ .

Unlike the potential of the metal, that of zeta cannot vary by applying a variable voltage.

3. Model and Simulation

3.1. Model calculation of Gouy-Chapman capacitance

In this section, the Gouy-Chapman model, based on Matlab routine, is used to calculate the capacitance at the interface of the electrode/electrolyte.

One purpose of this simulation is to determine the influence of the concentration of redox ions (I^-/I_3^-) on Gouy-Chapman capacity and its influence on the J-V curve for different variations of light shading frequency.

The following equation links the potential difference across the electrolyte ($\Phi(0) - \Phi^\infty$) to metal electrical charge density [16]:

$$\sigma^M = [8 \cdot C \cdot k \cdot T \cdot \epsilon_0 \cdot \epsilon_r]^{1/2} \cdot \sinh \left[\frac{e}{2 \cdot k \cdot T} (\Phi(0) - \Phi^\infty) \right] \quad (6)$$

σ^M : surface charge density [C/m^2];

C : volume ion density [C/m^3];

k : Boltzmann constant;

T : Ambient temperature [K];

ϵ_0 : The permittivity of vacuum;

ϵ_r : The relative permittivity of the medium;

$\Phi(0)$: internal potential of the solution at the point $x = 0$ [V];

Φ^∞ : internal potential of the solution at the point $x \rightarrow \infty$ [V].

$$\Phi(x) - \Phi^\infty = [\Phi(0) - \Phi^\infty] \cdot \exp(-K \cdot x) \quad (7)$$

with:

$$K = \left[\frac{2 \cdot C \cdot e^2}{\epsilon_0 \cdot \epsilon_r \cdot k \cdot T} \right]^{1/2} \quad (8)$$

From the equations (6) and (7), the capacity C_{gc} corresponding to the volume distribution of ions predicted by the Gouy-Chapman theory is defined as the derivative of the surface density of the charge with respect to the potential drop in solution[16].

$$C_{gc} = \frac{\partial \sigma^M}{\partial (\Phi(0) - \Phi^\infty)} = \left[\frac{2 \cdot C \cdot e^2 \cdot \epsilon_0 \cdot \epsilon_r}{kT} \right]^{1/2} \cdot \cosh \left[\frac{e}{2 \cdot k \cdot T} (\Phi(0) - \Phi^\infty) \right] \quad (9)$$

The C_{gc} capacity used in the simulation represents the equivalent capacitance calculated from the equation for the two ions redox (I^-/I_3^-).

3.2. Modelling of the PV generator (PVG)

The modeling of photovoltaic cells necessarily involves a judicious choice of equivalent circuits. To develop an accurate equivalent circuit for a PV cell, it is advisable to understand the physical configuration of the cell components as well as the electrical characteristics of each item. According to this philosophy, several analytical models are developed to represent a highly nonlinear behaviour of semiconductor junctions which are the basis of their achievements [17]. These models differ from each other by mathematical procedures and the number of parameters involved in the calculation of the voltage and current of the photovoltaic model.

Two models of PVG are introduced; namely [18]:

- Model with a diode (or single exponential)
 - Model with two diodes (or double exponential).
- Both are based on the well-known Shockley diode equation.

The functioning of a photovoltaic model is described by the standard model of a diode, established by Shockley, for a single PV cell (Figure 6) [18].

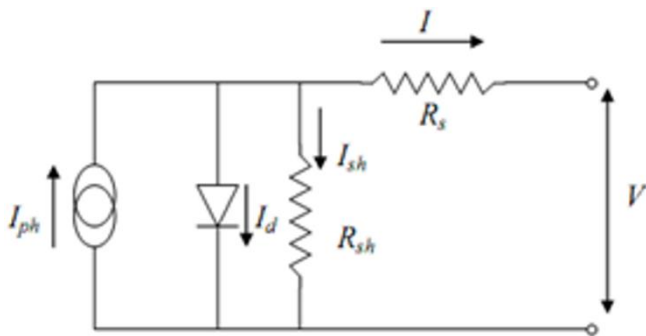


Fig. 6. Diagram of solar cell equivalent circuit; single diode model

The current provided by the cell is given by the equation (10).

$$I = -I_{ph} + \frac{V - R_s I}{R_{sh}} + I_s \left[\exp\left(\frac{q(V - R_s I)}{m k T}\right) - 1 \right] \quad (10)$$

- I: Current supplied by the cell [A]
- V: Voltage of the cell [V]
- I_{ph} : Photocurrent [A], proportional to the irradiance
- I_s : The diode saturation current [A], depending on the temperature [K]
- R_s : Series resistor [Ω].
- R_{sh} : Shunt resistor (or parallel) [Ω].
- q: Electron charge = $1.602 \cdot 10^{-19}$ Coulomb
- m: Quality factor of the diode, typically between 1 and 2.

Note that the two resistors R_s and R_{sh} depend on the development of the electrodes technology. R_s should be minimized; however R_{sh} should be maximized.

The photocurrent I_{ph} varies with light irradiation, it is determined in relation to the effective values of Φ and T compared with these of the reference conditions:

$$I_{ph} = \frac{\Phi}{\Phi_{ref}} \left[I_{ph_{ref}} + \mu_{Ics}(T - T_{ref}) \right] \quad (11)$$

Φ and Φ_{ref} : effective and reference irradiance [W/m^2].

T and T_{ref} : effective and reference temperature [K].

μ_{Ics} : photo-current temperature coefficient, is often given by the manufacturer, it is positive but very small.

The reference conditions Φ_{ref} , T_{ref} are specified to obtain the manufacturer's specifications (V_{oc} , I_{sc} , V_{max} , I_{max}). They are always given under STC (Standard test Conditions $1000 W/m^2$, $25^\circ C$, AM1.5 spectrum) or by experimental measurements.

By involving the C_{gc} , the electrical equivalent circuit of DSSC will correspond to the circuit of Figure 7.

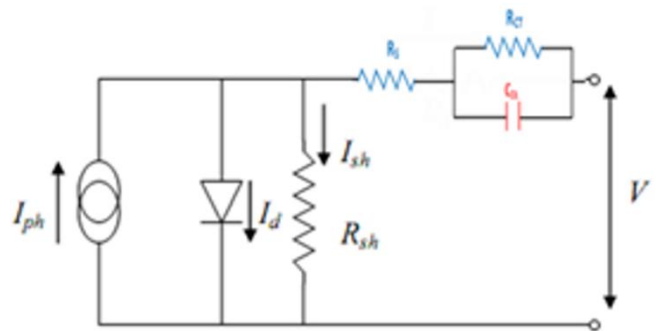


Fig. 7. Diagram of solar cell equivalent circuit; single diode model with Gouy-Chapman capacitor.

4. Results and discussion

4.1. The influence of the concentration of redox ions

Figure 8 represents the variation of potential at various redox ions concentrations of electrolyte in respect with distance from counter electrode. The surface potential is taken 0.75 eV. The figure shows that the potential extends up to a distance from the electrode in the order of nanometer. In this case the distance is about 1.4 nm. In addition, the decrease of the potential is proportional to the concentration of the redox ions (I^-/I_3^-) in the electrolyte which has the same role as the hole carriers in a standard diode. This result corresponds to the results published in [7].

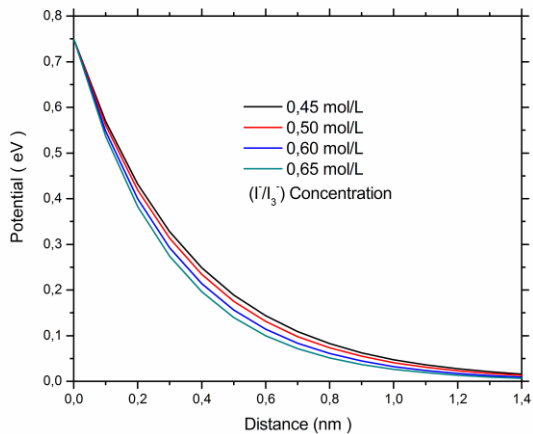


Fig.8. The variation of potential with double layer distance at various redox ions concentrations of electrolyte. Surface potential of 0.75 eV.

The following Figure shows the variation of the capacitance of Gouy-Chapman based on the potential for different concentrations of the redox ions.

The increase of the potential engenders an increasing in C_{gc} capacity. The variation in the capacitance is more outstanding for relatively high potential. According to equation (9) the C_{gc} capacity is closely related to the potential in the vicinity of the electrode of the solar cell and with the ion concentration of the electrolyte, similar results are obtained by Shapovalov [19].

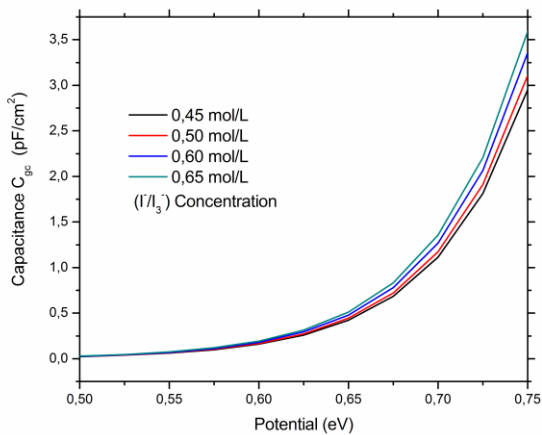


Fig. 9. The variation of Gouy-Chapman capacitance of the DSSC electrode with potential at different redox ions concentrations of electrolyte.

4.2. The influence of the capacity C_{gc} on the J-V curve

In this section the impact of C_{gc} on the J-V curve is studied; therefore J-V curves are plotted from equation (10) for various values of C_{gc} as illustrated in Figure 10.

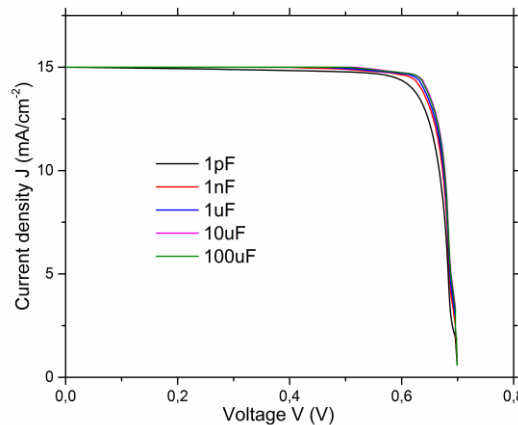
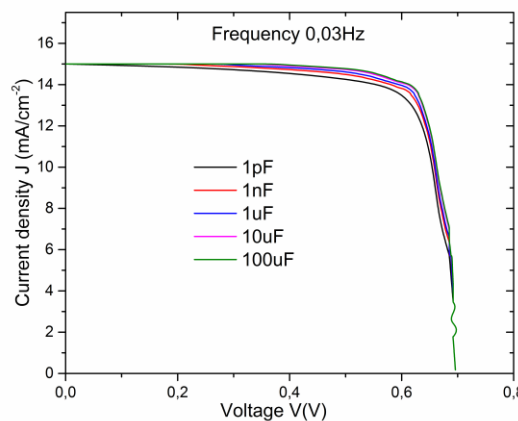


Fig.10. J-V curves for different values of C_{gc} .

For high values of C_{gc} ; 1 μ F, 10 μ F and 100 μ F, the Maximum Power Point (MPP) improves. The increase of the concentration of redox ions in the electrolyte leads to an augmentation in the Fill Factor (FF) therefore to the efficiency of the solar cell of about 10% without overflowing the Gouy-Chapman model.

4.3 The influence of the light flow shading frequency on the J-V curve

In this part, light will be shed on the behaviour of the dye cell towards fluctuations of light flow (which may be caused by the wind turbine blade shade; the case of wind solar hybrid system), which, in turn, cause fluctuations of the photo-generated current. A current generator (I_{ph} in Figure 7) was created by Matlab Simulink that generates photocurrents at different frequencies and forms. By varying the shading frequency, the J-V curves obtained are shown in Figure 11(a to d):



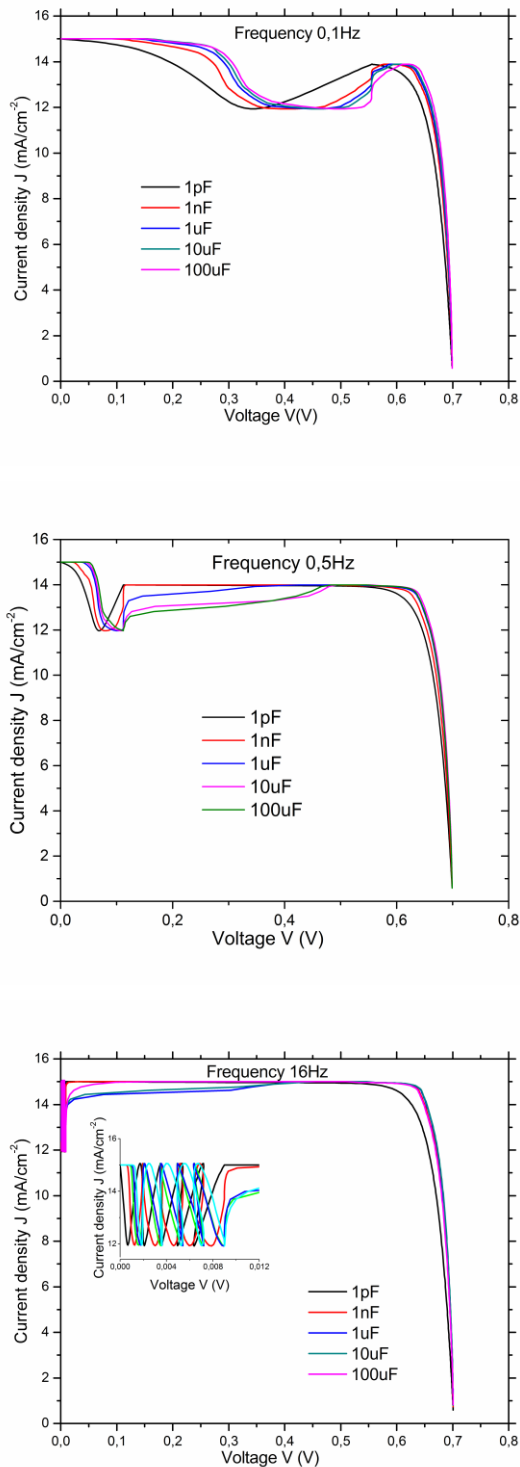


Fig.11. J–V curves for different frequency values of shading of light flow. a) 0.03 Hz, b) 0.1 Hz, c) 0.5 Hz, d) 16 Hz

According to the results the deterioration of the J–V curve increases with the increasing of shading frequency. The deformation of J–V curves slides towards the density current axis. These results agree remarkably well with experiment [20]. However, for the shading with a period greater than 30 seconds (a frequency $<0.03\text{Hz}$), the J–V curves remain unchanged.

5. Conclusion

In order to improve the performance of DSSCs cells, many materials, various designs and parameters have been studied. The influence of the concentration of redox ions (I^-/I_3^-) and C_{gc} capacity on the J–V curve have been opted for.

Increasing the concentrations of the redox ions in the electrolyte leads to increase the ability of the double layer transferring electrons. This increase in concentrations, in its turn, decreases the width of the region where the electrolyte field manifests.

For relatively high values of C_{gc} capacity the maximum power point improves. An increasing of 10% of efficiency is obtained varying C_{gc} from $1\mu\text{F}$ to $100\mu\text{F}$. These C_{gc} values comply with Gouy-Chapman model. The second part of this study reveals that the deterioration of the J–V curve increases with the increasing of the shading frequency of the incident light flow. However, for the shading frequency less than 0.03Hz , the J–V curves remain unchanged.

References

- [1] N. Marom, J. E. Moussa, X. Ren, A. Tkatchenko, and J. R. Chelikowsky, “Electronic structure of dye-sensitized TiO_2 clusters from many-body perturbation theory,” *Phys. Rev. B*, vol. 84, No. 24, p. 245115, 2011.
- [2] C. M. Lewandowski, N. Co-investigator, and C. M. Lewandowski, *Solar cells: materials, manufacture and operation*, Elsevier Ltd, vol. 1. 2015.
- [3] M. Onodera, R. Nagumo, R. Miura, A. Suzuki, H. Tsuboi, N. Hatakeyama, A. Endou, H. Takaba, M. Kubo, and A. Miyamoto, “Multiscale simulation of dye-sensitized solar cells considering schottky barrier effect at photoelectrode,” *Jpn. J. Appl. Phys.*, vol. 50, No. 4 PART 2, pp. 2–7, 2011.
- [4] K. Nithyanandam and R. Pitchumani, “Analysis and design of dye-sensitized solar cell,” *Sol. Energy*, vol. 86, No. 1, pp. 351–368, 2012.
- [5] J. Villanueva, J. A. Anta, E. Guille, G. Oskam, V. Uni, P. De Ola, and V. Se, “Numerical Simulation of the Current - Voltage Curve in Dye-Sensitized Solar Cells,” pp. 19722–19731, 2009.
- [6] A. Sedghi and H. Miankushki, “Influence of TiO_2 electrode properties on performance of dye-sensitized solar cells,” *Int J Electrochem Sci*, vol. 7, pp. 12078–12089, 2012.
- [7] J. M. Paz-garcia, B. Johannesson, L. M. Ottosen, and A. B. Ribeiro, “Modeling of Electric Double-Layers Including Chemical Reaction Effects,” *Electrochim. Acta*, vol. 150, pp. 263–268, 2014.
- [8] R. Boukenoui, H. Salhi, R. Bradai, and A. Mellit, “A new intelligent MPPT method for stand-alone photovoltaic systems operating under fast transient variations of shading patterns,” *Sol. Energy*, vol. 124, pp. 124–142, 2016.

- [9] F. Belhachat and C. Larbes, “ Modeling , analysis and comparison of solar photovoltaic array configurations under partial shading conditions,” *Sol. Energy*, vol. 120, pp. 399–418, 2015.
- [10] A.V. Delgado, F. Gonzalez-Caballero, R.J. Hunter, L.K. Koopal, J. Lyklema, Measurement and interpretation of electrokinetic phenomena, *J. Colloid Interf. Sci.* 309 (2) (2007) 194–224.
- [11] J. Kang, J. Wen, S. H. Jayaram, A. Yu, and X. Wang, “Development of an equivalent circuit model for electrochemical double layer capacitors (EDLCs) with distinct electrolytes,” *Electrochim. Acta*, vol. 115, pp. 587–598, 2014.
- [12] I. G. Bosco, I. S. Cole, and B. Emmanuel, “Regulation of Interfacial Chemistry by Coupled Reaction-Diffusion Processes in the Electrolyte: A Stiff Solution Dynamics Model for Corrosion and Passivity of Metals,” *J. Electroanal. Chem.*, vol. 722–723, pp. 68–77, 2014.
- [13] T. Jacob and L. Sabo, *Electrochemical Double Layer*. Elsevier Inc., 2015.
- [14] F. B. Moghadam and A. Mashreghi, “ Investigating the electrolyte iodine concentration effect on photovoltaic properties of dye-sensitized solar cells by electrochemical impedance spectroscopy,” *Mater. Sci. Semicond. Process.*, vol. 40, pp. 84–89, 2015.
- [15] K. B. Oldham, “A Gouy – Chapman – Stern model of the double layer at a (metal)/(ionic liquid) interface,” vol. 613, pp. 131–138, 2008.
- [16] Hubert H.G, “Electrochimie physique et analytique“, *Presse polytechnique et universitaires Romandes*, 2eme édition revue et augmentée, 2007, Suisse.
- [17] P. Junsangsri and F. Lombardi, “Modelling and extracting parameters of organic solar cells, *Electron.Lett*” vol. 46, No. 21, pp. 1462, 2010.
- [18] O. Gergaud, B. Multon, H. Ben Ahmed, “Analysis and Experimental Validation of Various Photovoltaic System Models”, 7th International ELECTRIMACS Congress, Montréal, August 2002.
- [19] V. L. Shapovalov, “The interaction of electric field and hydrostatic pressure in an electrical double layer : A simple “first principle” model that accounts for the finite sizes of counter ions,” *J. Colloid Interface Sci.*, vol. 454, pp. 187–191, 2015.
- [20] P. Bulanyi and R. Zhang, “Shading Analysis & Improvement for Distributed Residential Grid- Connected Photovoltaics Systems”, *The 52nd Annual Conference of the Australian Solar Council*, 2014.